

PSF-Radon transform algorithm: Measurement of the point-spread function from the Radon transform of the line-spread function

Sandra Martínez¹ and Oscar E. Martínez¹

¹Universidad de Buenos Aires

March 26, 2024

Abstract

In this article we present a new method called PSF-Radon transform algorithm. This algorithm consists on recovering the instrument point spread function (PSF) from the Radon transform (in the line direction axis) of the Line Spread function (that is, the image of a line). We present the method and tested with synthetic images, and real images from macro lens camera and microscopy. A stand-alone program along with a tutorial is available, for any interested user, in [?] .

PSF-Radon transform algorithm: Measurement of the point-spread function from the Radon transform of the line-spread function

SANDRA MARTÍNEZ^{1,*} AND OSCAR E. MARTÍNEZ²

¹Departamento de Matemática, FCEyN-UBA and IMAS, CONICET, Buenos Aires, Argentina

²Laboratorio de Fotónica, Instituto de Ingeniería Biomédica, FI-UBA, CONICET, Buenos Aires, Argentina

*smartin@dm.uba.ar

Compiled November 28, 2023

In this article we present a new method called PSF-Radon transform algorithm. This algorithm consists on recovering the instrument point spread function (PSF) from the Radon transform (in the line direction axis) of the Line Spread function (that is, the image of a line). We present the method and tested with synthetic images, and real images from macro lens camera and microscopy. A stand-alone program along with a tutorial is available, for any interested user, in [1].

Keywords: Image Resolution, Point Spread Function, Line Spread Function, Radon transform, Microscopy.

<http://dx.doi.org/XXXX>

1. INTRODUCTION

Determining the instrument point spread function (PSF) has been accepted for a long time [2] as a key issue when assessing the quality of the image and is crucial for determining the resolution in any microscopy technique based on fluorescence, with or without super-resolution. This information indicates what features of the object under study will be distinguished (image resolution). It is a well established technique to measure the PSF imaging a point-like source such as a very small bead. The bead size must be between 10% and 40% of the size of the PSF width not to distort significantly the measurement [3, 4]. A measurement within a 1% accuracy would require a bead of about 10% of the PSF width, which would involve beads so small that the noise in the measurement would hinder the possibility of a reliable measurement. Precise PSF determinations are mandatory if image improvement is performed numerically by deconvolution [5–8]. Moreover a recent deconvolution method has been presented [9] that overcomes the ill posed problem allowing a three to fivefold increase in the resolution, but has been shown to require a precise knowledge of the PSF better than 3% [10]. To overcome this difficulty theoretical estimation of the PSF has been a way to try to circumvent the problem and each specific microscopy technique requires the derivation of peculiar analytical or numerical expressions for the PSF. For a confocal microscope different theoretical calculations have been proposed and they will depend on the Airy iris used at the detection [11–13] and eventual filters [14]. For a light sheet experiment the axial profile will be that of the pump beam transverse profile, typically a Gaussian or Bessel beam and the angle used for collection, and specific PSF calculators have been derived [15]. Size of the bead to measure the PSF has been shown to be critical and a protocol for the 3D PSF measurement is well established [3] and it indicates that a smooth symmetric axial profile is achieved. Gaussian approximations for confocal microscope PSF have been proposed [16] or eventually more complex analytical expression involving superposition of Gaussian functions [12] or Bessel functions [13]. Multiphoton microscopes provide another axial stacking method and multiparametric Gaussian fittings have proven a valuable approximation to the 3D PSF [17, 18]. New methods and geometry appear continuously with increasing resolution and a reliable way to measure the PSF in a precise manner is a pending subject. A way around this is to design specific patterned samples to provide ways of assessing the instrument resolution and accuracy such as the Argolight sample [19] for AiryScan, confocal, structured illumination and other fluorescent microscopy techniques or origami labelled DNA samples [20] for very high super-resolution methods. In this work we present a method that reconstructs the PSF from the image of a line, i.e., the Line Spread Function (LSF) [2].

The method starts with the measurement of an image of a line. Then the algorithm determines the angle of inclination and performs the Radon transform in that direction, assuming radiality of the PSF, this Radon transform is used as the Radon transform of the PSF. Finally the Radon inversion formula is calculated obtaining a numerical expression of the PSF.

One of the main advantages of this method is that the line, compared to a small bead, requires much less exposure time to achieve the same signal to noise levels. The second point is that the retrieval of the method consists on numerical expressions for the PSF, that

is, a matrix containing the values of the PSF. In this way, the method does not require having to adjust it by an analytical function, as needed when retrieving the PSF from a noisy measurement from a very small bead.

The article is organized as follows. In Section 2 we describe the steps of the method. We divided this section in 3 subsections where in A we define the Radon transform and show how we use the LPS to determine the PSF when knowing the correct angle, in B we describe how we determine the angle of the line, in Section C we describe how we symmetrize the Radon transform in the presence of noise and summarize the algorithm.

Section 3 is devoted to test our methods in 3 cases. In Section A we analyze synthetic images and discuss how the error in the angle and photon count noise affects the performance of the method (Subsections A.1 and A.1). Experimental results for macro lens camera are shown in Section B where we also present in B.2 a new method that consists on applying Radon-PSF algorithm for the gradient of a step image. Finally in Section C we apply the algorithm to determine the PSF for fluorescence microscopy images.

Additionally Appendix 5 is devoted to: the description of how we remove, when present, the background and Salt & Pepper noise (A) and how we recover the Radon transform of the LSF when the structure consists on two or more lines (B). A self-contained tutorial on how to use the provided program is available in [1].

2. DESCRIPTION OF METHOD

A. Recovering the PSF using the Radon transform: theoretical description

Let f be the function we want to retrieve (i.e. the PSF). If we define the segment $x \cos \theta + y \sin \theta = r$, where r is the distance from the line to the origin and θ is the angle of the line from the x -axis, the Radon transform of f is defined by,

$$\mathcal{R}[f](\theta, r) = \int_{-\infty}^{\infty} \int_{-\infty}^{\infty} f(x, y) \delta(x \cos \theta + y \sin \theta - r) dx dy \quad (1)$$

On the other hand, we have by the filter back projection Theorem ([21, 22]) the following Radon inversion formula,

$$f(x, y) = \frac{1}{2\pi} \int_0^\pi (\mathcal{R}[f](\theta, \cdot) * h)(x \cos \theta + y \sin \theta) d\theta \quad (2)$$

where h satisfies $\hat{h}(\omega) = |\omega|$. Here $*$ represents the convolution operator and $\hat{\cdot}$ the Fourier transform.

If f is radially symmetric then for all θ , $\mathcal{R}[f](\theta, r) = \mathcal{R}[f](0, r)$, therefore to recover f using Radon inversion formula, it is enough to calculate $\mathcal{R}[f](0, s)$ (that is, the projection on the x axis).

If we define $g(x, y) = f * \delta_x$, where $\delta_x(x, y)$ is the segment $x = 0, y \in [-L/2, L/2]$, therefore the Line Spread Function (LSF) is defined as in [2] by,

$$g(x, y) = \int_{-L/2}^{L/2} f(x, y - y') dy' \quad (3)$$

and then

$$\mathcal{R}[g](0, r) = \int_{-\infty}^{\infty} g(r, y) dy = \int_{-\infty}^{\infty} \int_{-L/2}^{L/2} f(s, y - y') dy' dy = L \int_{-\infty}^{\infty} f(r, y) dy = L\mathcal{R}[f](0, r). \quad (4)$$

That means that we can recover the radon transform of the PSF from the Radon transform of the LSF. This Radon transform results in a function L times more intense than the Radon transform of the PSF, which is an advantage when dealing with noisy images. See Figure 1a for an example of a LSF, Figure 1b for its Radon transform in the direction of the line and Figure 1c for the PSF obtained after applying the inverse transform.

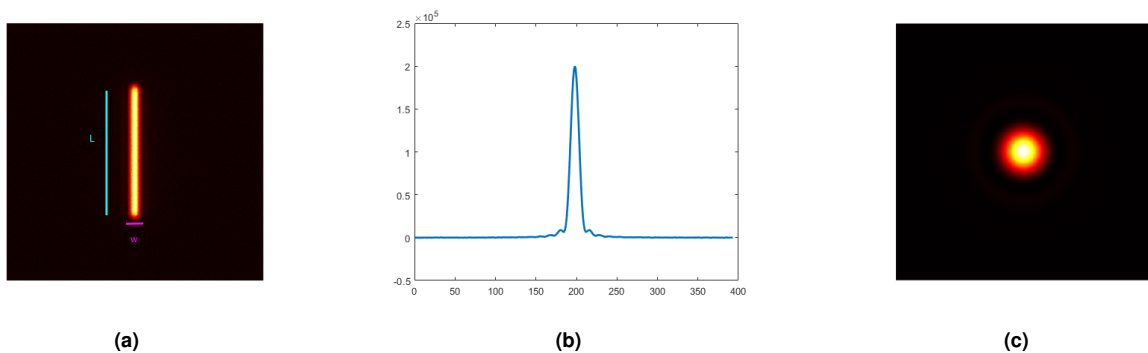


Fig. 1. PSF- Radon transform algorithm. (a) original image of a LSF (g in Eq. (3)). (b) Radon transform in the direction of the LSF ($\mathcal{R}(g)$ in Eq. (4)). (c): PSF obtained after applying the inverse transform.

Remark 2.1 In practice the integral of g will be taken in a finite interval $[-B/2, B/2]$. If we choose B sufficiently large, i.e. $B \gg L + \text{FWHM}(f)$, we obtain,

$$\int_{-B/2}^{B/2} g(r, y) dy = \int_{-L/2}^{L/2} \int_{-B/2-y'}^{B/2-y'} f(r, u) du dy' \rightarrow L \int_{-\infty}^{\infty} f(r, y) dy \quad \text{if } B \rightarrow \infty \quad (5)$$

73 Analogously, if $L \gg B + \text{FWHM}(f)$,

$$\int_{-B/2}^{B/2} g(r, y) dy \rightarrow B \int_{-\infty}^{\infty} f(r, y) dy \quad \text{if } L \rightarrow \infty \quad (6)$$

74 Here FWHM represents the Full width at half maximum of the function f . The Eq. (4), Eq. (5), Eq. (6) tells us that the Radon transforms of f
75 and g are equal with the difference that the intensity of the last one is multiplied by the length of the segment (case of Eq. (5)) or the zone where g is
76 projected (case Eq. (6)). The method consist then, on recovering f from the Radon transform of g , using the formula given in Eq. (2).

77 See the figures in the tutorial at [1] to see a scheme of how the images should be cropped.

78 B. Error in the angle - finding the angle

79 In practical experiments the orientation of the image is arbitrary. For that reason, the first step of the algorithm consists on determining
80 that angle.

81 Assume that f is a Gaussian function, and the segment has an inclination of θ degrees, that is, if we make the change of variables
82 $x = -vs + uc$, $y = us + vc$, with $c = \cos(\theta)$, $s = \sin(\theta)$, we define the resulting inclined image as $\tilde{g}(u, v) = g(x, y)$. If we calculate the
83 Radon transform of \tilde{g} with angle zero, we obtain

$$\mathcal{R}[\tilde{g}](0, u) = \frac{1}{2\pi\sigma^2} \int_{-L/2}^{L/2} e^{-\frac{(u-y/s)^2}{2\sigma^2}} \left(\int_{-\infty}^{\infty} e^{-\frac{(v-y'/c)^2}{2\sigma^2}} dv \right) dy' = \frac{1}{\sqrt{2\pi}\sigma} \int_{-L/2}^{L/2} e^{-\frac{(u-y/s)^2}{2\sigma^2}} dy' := F(u). \quad (7)$$

84 Observe that if $s = 0$ (no inclination) $\mathcal{R}[\tilde{g}](0, u) = L \frac{1}{\sqrt{2\pi}\sigma} e^{-\frac{u^2}{2\sigma^2}}$ and we recover the PSF as in the general case. In the case $s \neq 0$ we
85 have taking $r = \frac{y's}{\sigma}$, $\tilde{u} = \frac{u}{\sigma}$ and $\varepsilon = \frac{Ls}{2\sigma}$

$$h(u) := \frac{1}{L} F(u) = \frac{1}{L} \frac{1}{\sqrt{2\pi}\sigma} \int_{-L/2}^{L/2} e^{-\frac{(u-y/s)^2}{2\sigma^2}} dy' = \frac{1}{\sigma\sqrt{2\pi}2\varepsilon} \int_{-\varepsilon}^{\varepsilon} e^{-\frac{(\tilde{u}-r)^2}{2}} dr \quad (8)$$

86 We have the following $\int_{-\infty}^{\infty} h(u) du = 1$, $\int_{-\infty}^{\infty} h(u)u du = 0$, and taking $z = \tilde{u} - r$, $du = \sigma dz$

$$\int_{-\infty}^{\infty} h(u)u^2 du = \frac{1}{2\varepsilon} \int_{-\varepsilon}^{\varepsilon} \frac{1}{\sqrt{2\pi}} \int_{-\infty}^{\infty} e^{-\frac{z^2}{2}} (z+r)^2 \sigma^2 dz dr = \sigma^2 (1 + \varepsilon^2/3). \quad (9)$$

87 Therefore, if we assume $\varepsilon \ll 0$ the relative error of deviation between $h(u)$ and the PSF results,

$$\frac{\sigma - \sigma\sqrt{1 + \varepsilon^2/3}}{\sigma} = \frac{\varepsilon^2/3}{1 + \sqrt{1 + \varepsilon^2/3}} \sim \varepsilon^2/6 = \frac{1}{24} \left(\frac{L \sin(\theta)}{\sigma} \right)^2 \sim \frac{1}{24} \left(\frac{L\theta}{\sigma} \right)^2. \quad (10)$$

88 therefore, to obtain a relative error in the FWHM (or σ) less that $\Delta\sigma$ we need to detect the angle in a grid with step size

$$\Delta\theta \leq 24\sqrt{(\Delta\sigma)\frac{\sigma}{L}}. \quad (11)$$

89 Therefore it is necessary to have an estimate of the height and width of the segment, where the last one is comparable to the full width
90 at half maximum (FWHM) of the PSF. When the angle has the direction of the line, the FWHM of the Radon transform is minimum.
Therefore, the algorithm to detect the angle of the image is the following,

Algorithm 1. Image Angle

- 1: **procedure** ANGLE(*Image, rel_error*) ▷ image of a segment
- 2: For a given angle $\Delta\theta$, calculate for each $\theta = 0 : \Delta\theta : \pi$ the Radon transform and $p(\theta)$ the width of the peak.
- 3: Set: $w = \min p$, $L = \max p$.
- 4: Refine $\Delta\theta$ according with Eq. (11) with $\Delta\sigma = \text{rel_error}$.
- 5: Return to step 2.
- 6: **return** θ

91 In Figure 2 there is an example of a line inclined a certain angle, and how we define the width of the peak.
92

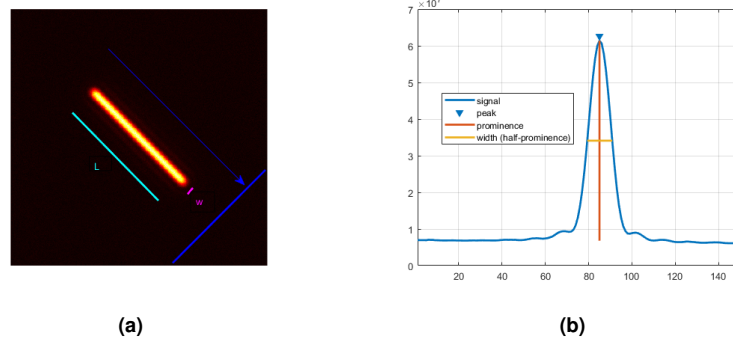


Fig. 2. Determination of the angular inclination. (a) line with 45° of inclination. (b) Radon transform for $\theta = 45^\circ$, peak, prominence and width.

C. Symmetrization of the Radon transform and PSF-Radon Algorithm

The main assumption of the method is that the PSF is radially symmetric and in consequence, its Radon transform is symmetric. But, in practice, the Radon transform of the image may have some fluctuations that made it non symmetric. This effect is due to distortion of the PSF or to the presence of noise. For that reason it was necessary to add a step to our method that consists on the symmetrization of the Radon transform (R). This symmetrization R_{sym} , consists on searching for the position of the peak of R , x_p , and taking the mean values between the two branches, that is, $R_{sym}(x) = \frac{1}{2}(R(x - x_p) + R(-x + x_p))$. Finally we take R_{sym} as an approximation of Radon transform (observe that in case R is already symmetric $R_{sym}(x) = R(x - x_p)$).

The complete steps of the method are summarized in Algorithm 2.

Algorithm 2. PSFRadon

- 1: **procedure** PSF(*Image*) ▷ image of a segment
- 2: Calculate the angle θ
- 3: R : Calculate the Radon transform of the image in the direction of θ .
- 4: $R \leftarrow$ Symmetrize the Radon transform.
- 5: $RR \leftarrow$ Make a matrix of 180 copies of R .
- 6: $PSF_{matrix} \leftarrow$ Calculate the Filtered Backprojection of RR .
- 7: **return** PSF_{matrix} ▷ A matrix containing the values of the PSF on the original grid.

3. EXAMPLES: SYNTHETIC AND REAL IMAGES

A. Synthetic images

A.1. Angle

To test the theoretical bound in Eq. (10) for more realistic cases, we constructed synthetic images convolving the line with a PSF consisting on the square of an Airy function (see Figure 3a). Along this article we will denote this PSF as Airy2. The parameters in Figure 3a are $L = 200$ px and $w = 10$ px. We approximated the PSF using the PSF- Radon algorithm with different errors in the angle of inclination. The resulting PSFs are plotted in Figure 3b. We obtained relative errors of the FWHM of 0.68, 0.26, 0.053, 2×10^{-4} when the errors in the angle were 5.4° , 3.6° , 1.8° , 0.18° , respectively. These results are consistent with the theoretical bound of the relative error of the FWHM for a Gaussian PSF which are 0.5863, 0.26, 0.065, 7×10^{-4} , respectively. Observe that when the error in the angle is less than 2° the differences between the PSF-Radon functions and the original Airy2 function are imperceptible (Figure 3b). It is important to observe that as the error in the angle grows the first thing that is lost is the information around the halo (Figure 3c).

A.2. Noise

To test how the noise affects the retrieval of the PSF- Radon function we designed a family of synthetic line-PSF images where Poisson noise was added. In Figure 4 there are two examples for different noise levels.

We conclude that the algorithm can be applied even when the image has high levels of noise. The only observation is that, as we increase the noise level some minor problems appear around the peak of the PSF.

B. Measurement of point-spread function for macro lens camera images

The first experimental test of the PSF-Radon algorithm was performed by taking pictures of a cell phone screen using a 5Mpixel camera with a macro lens with an iris to adjust the PSF. The images were taken at a camera-screen distance of 45cm. The iris of the camera was closed until we achieve a resolution of 12 pixels of the camera.

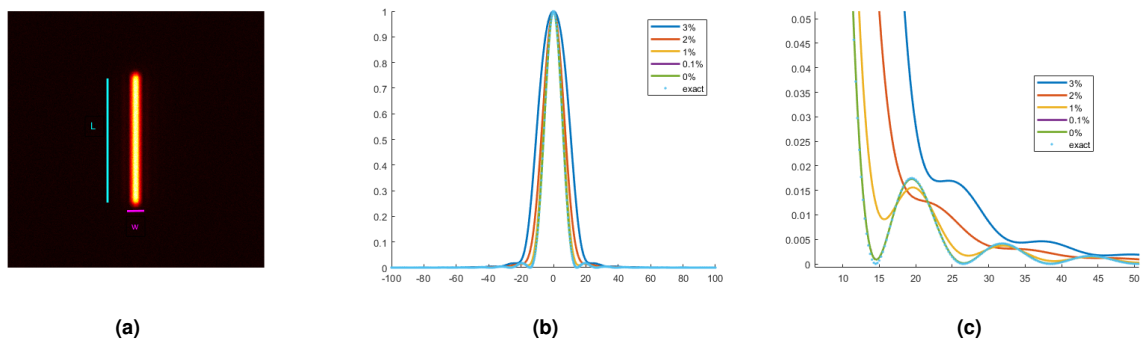


Fig. 3. PSF Radon using synthetic LSF function calculated for different errors in the inclination angle. (a) original vertical line. (b) PSF obtained with different errors in the angle. (c) zoom around the halo.

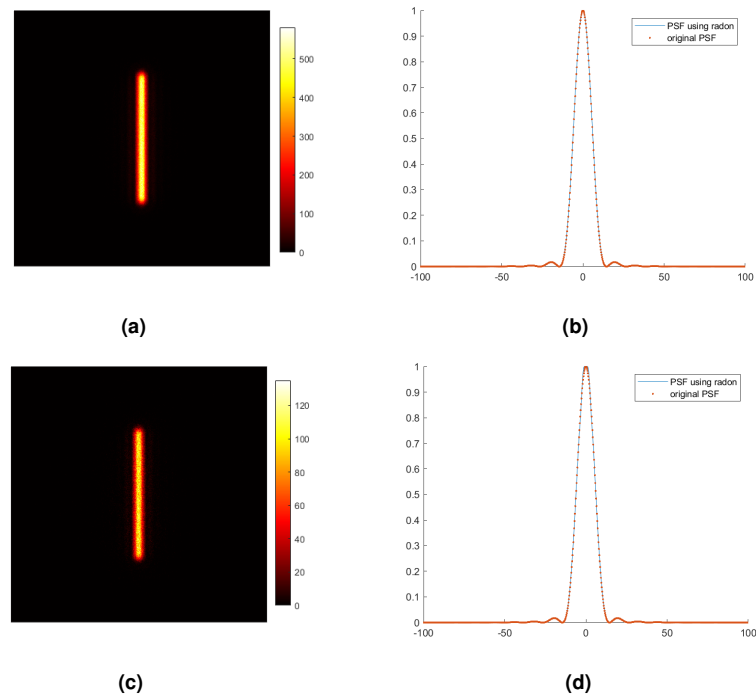


Fig. 4. First column, Top to bottom: Synthetic segment with different noise levels. Second column PSF obtained after applying the PSF-Radon algorithm together with the original PSF.

121 **B.1. PSF- Radon algorithm vs Fitting beads**

122 Figures 5a and 5b correspond to pictures of structures consisting on vertical, horizontal lines and beads, both structures (lines and
 123 beads) were built in such a way that the width in the camera are 3px , that is 25% lower than the resolution, in the first case the time
 124 exposure was of 0.5 seconds while in the second case this time was of 10 seconds. For these particular acquisitions it was necessary to
 125 remove the Salt & Pepper noise (for the details on how we attack this problem see Appendix A). Figure 5c corresponds to a zoom of a
 126 bead for the 0.5 seconds exposure time picture. Observe that due to the noise, all the information about the PSF is lost in this picture.
 127 After increasing the exposure time up to 10 seconds (Figure 5d) it is possible to recover, as in [3], the information of the PSF assuming a
 128 form to approximate the bead by a Gaussian function. On the other hand, in Figure 5e there is a zoom of the line obtained from Figure
 129 5a. In Figure 5f we made a comparison between the PSF obtained using the bead and the PSF-Radon algorithm. Observe that, despite
 130 the fact that the image of the line used for our method was acquired with a factor 20 lower of exposure time than the one that uses the
 131 beads, we were able to better recover the structure of the PSF. The presence of the halos can be appreciated with our method.

132 **B.2. Measurement of point-spread function using a step**

133 There exists another type of structure that can be used to determine the PSF that consists on using a step sample instead of a line.
 134 In the image this structure will have the form $\text{Step}(x, y) = f * H$, where H is a function that is equal to one when $0 \leq x \leq M$ and
 135 $-L/2 \leq y \leq L/2$ (see the rectangle in Figure 6a and zoom in 6c). If we calculate the partial derivative of Step in the x - direction we

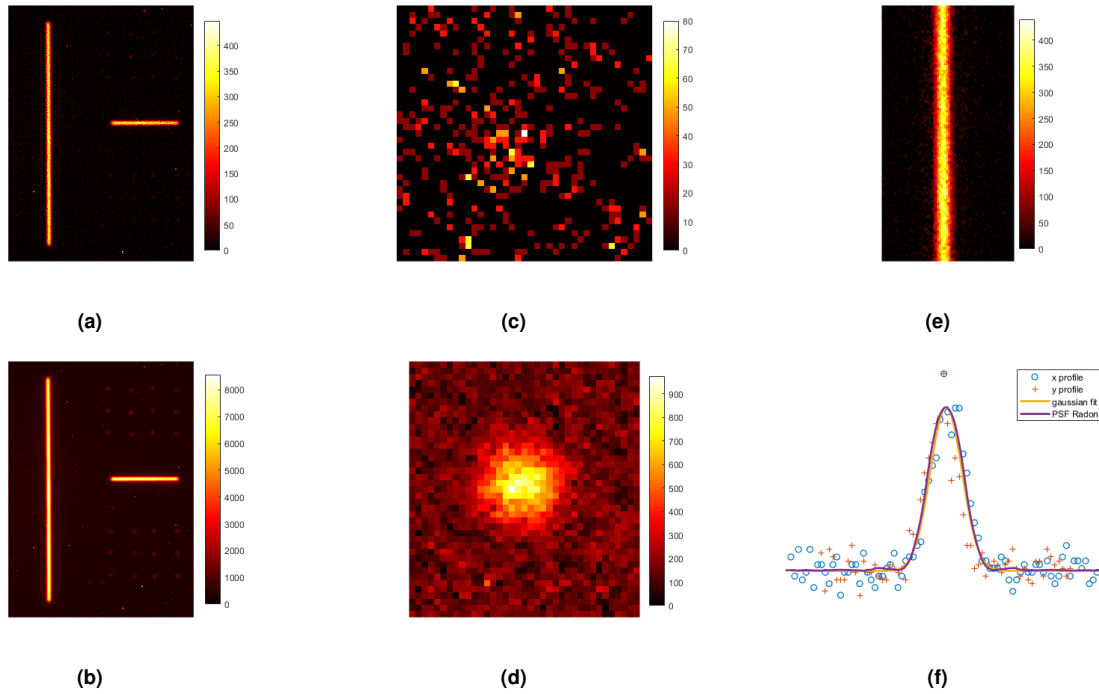


Fig. 5. (a) and (b): Acquisition with a standard camera of an image of a screen consisting on vertical, horizontal segments and beads (right top and bottom of the screen). Both the segments and the beads have a width of $3px = 25\%$ the resolution. In (a) the acquisition was taken with 0.5 seconds of time exposure, (b) with 10 seconds. (c) and (d) corresponds to a zoom of one of the beads in (a) and (b), respectively. (e) is a zoom of the vertical segment in (a). (f) comparison between the PSF obtained after applying the PSF- Radon algorithm from image (e) with the fitted Gaussian obtained from (d) together with its profiles in the x and y-axis.

136 obtain,

$$\frac{\partial Step}{\partial x}(x, y) = f * \frac{\partial H}{\partial x} = f * \delta_x(x, y) = g(x, y) \quad (12)$$

137 where g has the form defined in Eq. (3) (see Figure 6d).

138 To test the performance of this variant of the PSF-Radon algorithm we take again pictures of a screen, as in Section B, with structures
 139 consisting on rectangles and lines. Both structures are present in the same picture, Figure 6a. To compare both methods we use for the
 140 line the zone in Figure 6b and for the step the zone in Figure 6c. When the step has an inclination, the derivative must be taken in the
 141 direction perpendicular to the line (Figure 6d). The comparison between both resulting PSFs are plotted in Figure 6e.

142 C. Argolight: measurement of point-spread function for fluorescence microscopy

143 We also studied the performance of the PSF-Radon algorithm for microscopy images. We acquired images of an Argolight- SIM
 144 calibration sample that has multiple fluorescent reference standards with multiple geometric patterns designed for the quality control
 145 of microscopes, [23]. One of the patterns available in the sample is made up of gradually spaced lines. This pattern consists of pairs of
 146 $36 \mu m$ long lines whose spacing gradually increases from 0 nm to 390 nm, with a step of 30 nm (see Figure 7a).

147 An IX71 Olympus inverted microscope was used with an external 2X telescope in a 4f configuration before the camera (lateral port)
 148 to increase the magnification. A $60\times$ oil immersion objective was used with a $NA = 1.45$, that was reduced to the value indicated in
 149 each experiment by placing an iris in the conjugate plane between the lenses of the $2\times$ telescope. The sample was excited with an
 150 UV-LED and observed with a filter centered at 460 nm. A low noise CMOS camera (Andor Zyla 5.5) with $6.5 \mu m$ pixel size was used
 151 for image acquisition.

152 The reason why we add an iris to the lenses was that the sample has a non-negligible thickness in the axial direction (according to
 153 the manufacturer the thickness is $(600 \pm 200) nm$). Hence this sample cannot be used for high NA objectives as the out of focus signal
 154 would blur the PSF determination. Therefore, the iris allows the numerical aperture of the system to be modified to guarantee that the
 155 depth of focus of the optical system is greater than the thickness of the structure. The resulting numerical aperture is $NA \sim 0.55$.

156 Before applying the PSF-Radon algorithm, for this particular acquisition it was necessary to remove the background and the Salt
 157 & Pepper noise (for the details on how we attack these problems see Appendix A). Since this sample does not have any structure
 158 composed of an isolated line we have to adapt our algorithm to obtain the Radon transform of the LSF from what we call a 3 lines SF
 159 (see Figure 7b where the structure of the 3 lines can be visualized). For the details see Appendix B. In Figure 7c we plotted the 3 steps
 160 described in Algorithm 4 used to recover the Radon transform of the LSF. Finally, in Figure 7d we plotted the profile of the obtained
 161 PSF which results on having a resolution of $4.9px = 400nm$.

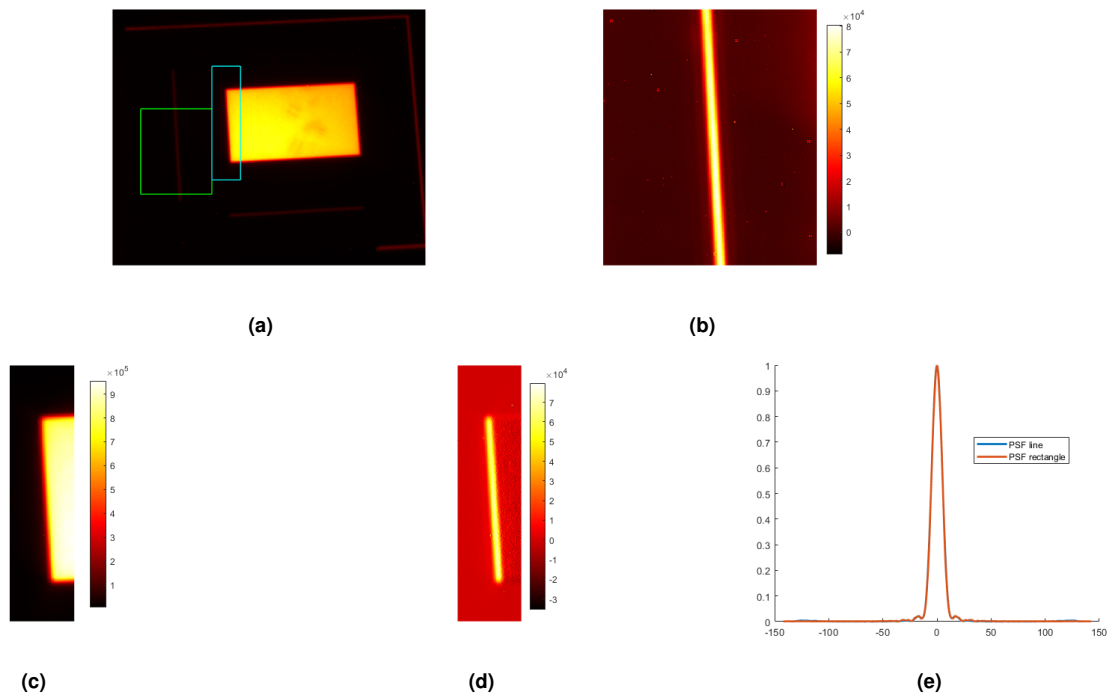


Fig. 6. (a): Original image. (b): zoom of the line (marked in green in (a)). (c): zoom of the step (marked in blue sky in (a)) and (d) represents the derivative of (c) in the direction perpendicular to the line. (e): comparison between the resulting PSFs.

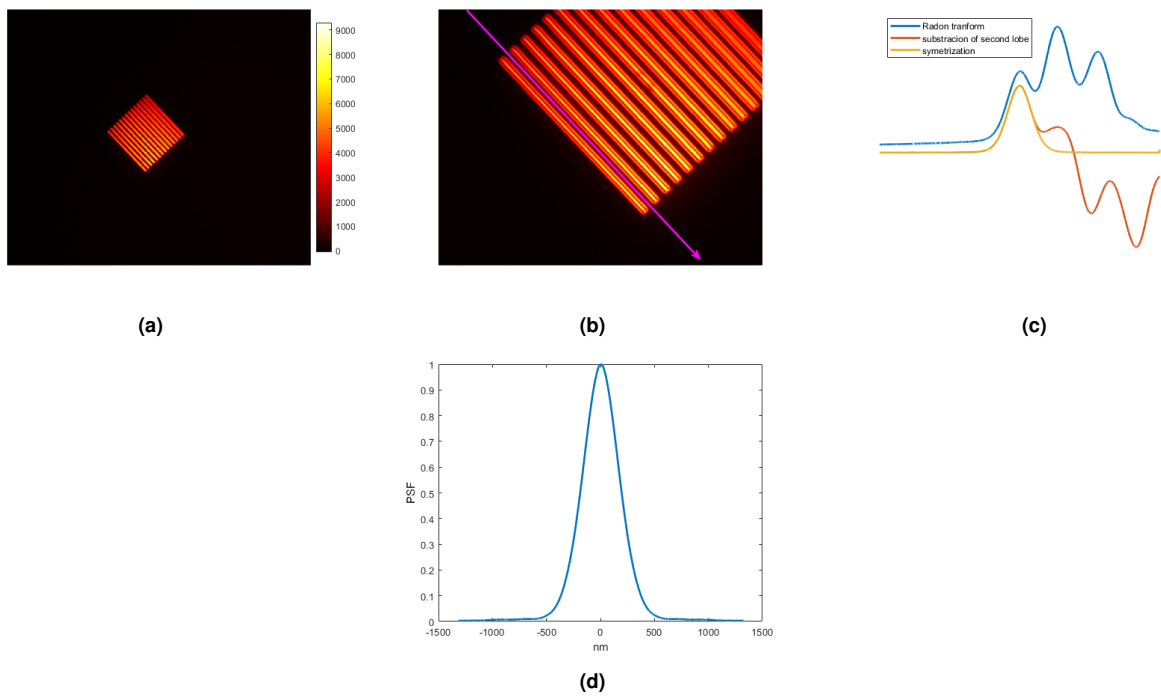


Fig. 7. (a): Original image consisting on several parallel lines. (b): zoom of the zone of interest (the arrow describes the angle used for the Radon Transform and the limit of the area used for the algorithm). (c): description of the steps used in Algorithm 4 (Radon transform (blue), subtraction of the second lobe (red) and approximation of the Radon transform of the LSF (yellow)). (d): Resulting PSF.

162 **4. CONCLUSIONS**

163 In this article we presented a new method called PSF-Radon transform algorithm that consists on recovering the instrument point
 164 spread function (PSF) from the Radon transform (in the line direction axis) of the Line Spread function. We presented the description

165 and theory of the method. Also we developed an algorithm for finding accurately the angle of inclination of the line and we gave
 166 a theoretical prove of how the PSF is affected if we obtain this angle with a certain error. We tested the method first in synthetic
 167 images, showing how the accuracy in the angle of inclination and the Poisson noise affects the retrieval of the PSF. We also tested the
 168 method on real images from macro lens camera and microscopy and we developed an alternative method consisting on applying the
 169 PSF-Radon method to the directional derivative of the image of a step.

170 We conclude that the main advantages of this method is that the line, compared to a noisy measurement from a very small bead,
 171 requires much less exposure time to achieve the same signal to noise levels and does not requires having to adjust the PSF by a
 172 analytical function to overcome the noise uncertainties.

173 A stand-alone program along with a tutorial is available in [1], hoping that this method will be very useful for anyone interested
 174 in characterizing the PSF of their system.

175 Work is in progress on developing new methods to build line and step structures to replace fluorescent beads, being a trivial one to
 176 use sharp knife edge structures for transmission and reflection microscopes.

177 5. APPENDIX

178 A. Removing background and Salt & Pepper Noise

179 In many measurements the inclination together with a background (like in Figure 8a) may cause distortions in the Radon transform
 180 (see Figure 8b). For that reason we define a function that performs the histogram of the image and uses the maximum of this histogram
 181 as an estimation of the background (see Figure 8c) and subtracts it. As we can observe in Figure 8d, for this synthetic image the
 182 resulting PSF has a distortion both near the peak and around the halo if we do not subtract the background (Figure 8e and Figure 8f).
 As noise levels increases, failure to make this correction could lead to incorrect approximations of the PSF.

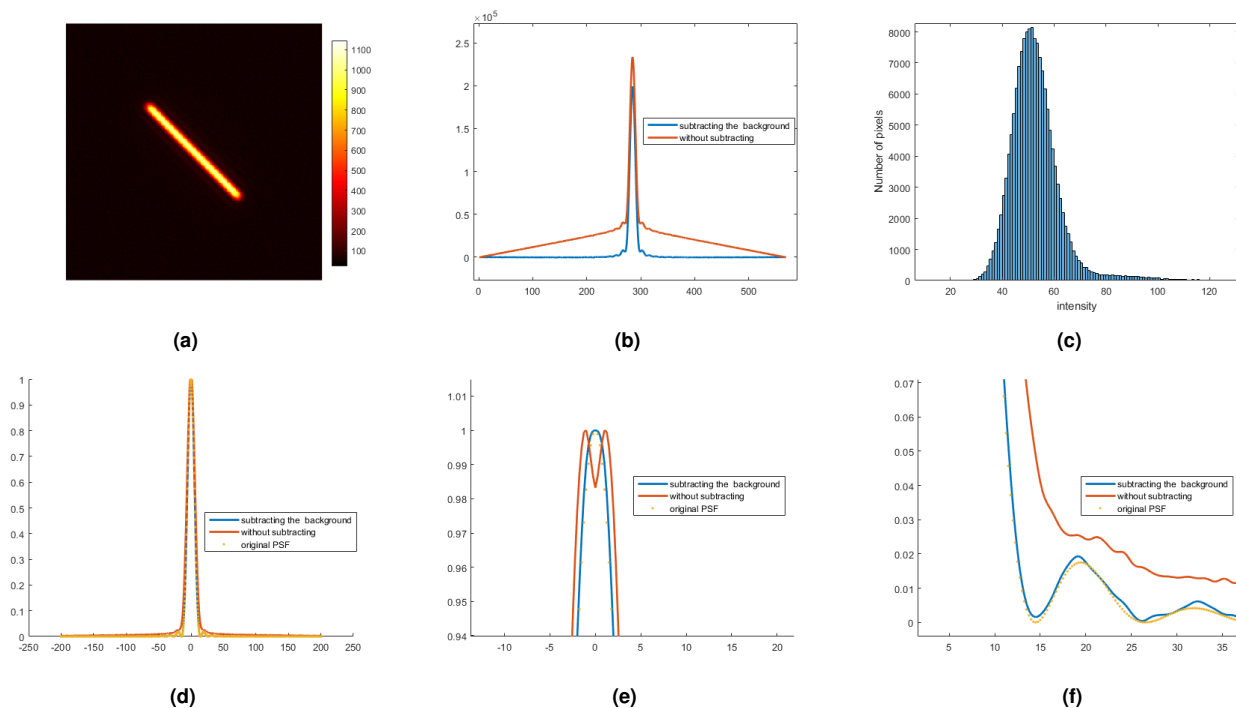


Fig. 8. (a) : Synthetic image of a line-PSf with a 45° of inclination, with a background= 50 and with Poisson noise (maximum intensity= 1000). (b): Radon transform of the image using the subtract background function and without using it. (c) histogram of the image showing a peak around the background. (d) profile of the PSF- Radon functions obtained using the Radon transforms of (c). (e) and (f) are zooms in different regions of plot (c).

183 Another type of noise may appear due to the image transmission channels. That is, an impulsive noise that causes the affected
 184 pixels to take an extreme value, that is, maximum (white) or minimum (black). The effect of this noise on grayscale image is to have
 185 various black and white dots scattered randomly throughout the image, named Salt and Pepper noise (see Figure 9a).

186 This Salt and Pepper noise can affect the performance of the PSF- Radon algorithm, see Figures 9b and 9c. To solve this noise, it
 187 is standard to use spatial average filters, but since this filter converts the original image to a blurred one the result is a loss in the
 188 resolution, that is a change in the PSF.

189 For that reason we solve this problems using Algorithm 3,
 190

Algorithm 3. Remove Salt & Pepper

- 1: **procedure** OUTPUT IMAGE (INPUT IMAGE, M)
- 2: Calculate the histogram of INPUT IMAGE.
- 3: z_1 : Search for the first zero on the right side of the histogram.
- 4: Salt pixels: Search for all the pixels with bin intensities two positions to the right of z_1 .
- 5: **return** OUTPUT IMAGE: Each output salt pixel contains the median value in the $M \times M$ neighbourhood, without taking the value of the current pixel, around the corresponding salt pixel in INPUT IMAGE.

191 A picture and the result of this algorithm is describe in Figure 10.

192 **Remark 5.1** For our problem the pepper pixels where not critical. In the case that it was necessary to remove also these pixels it can by applied a
 193 similar algorithm by detecting for the first zero on the left side of the histogram.

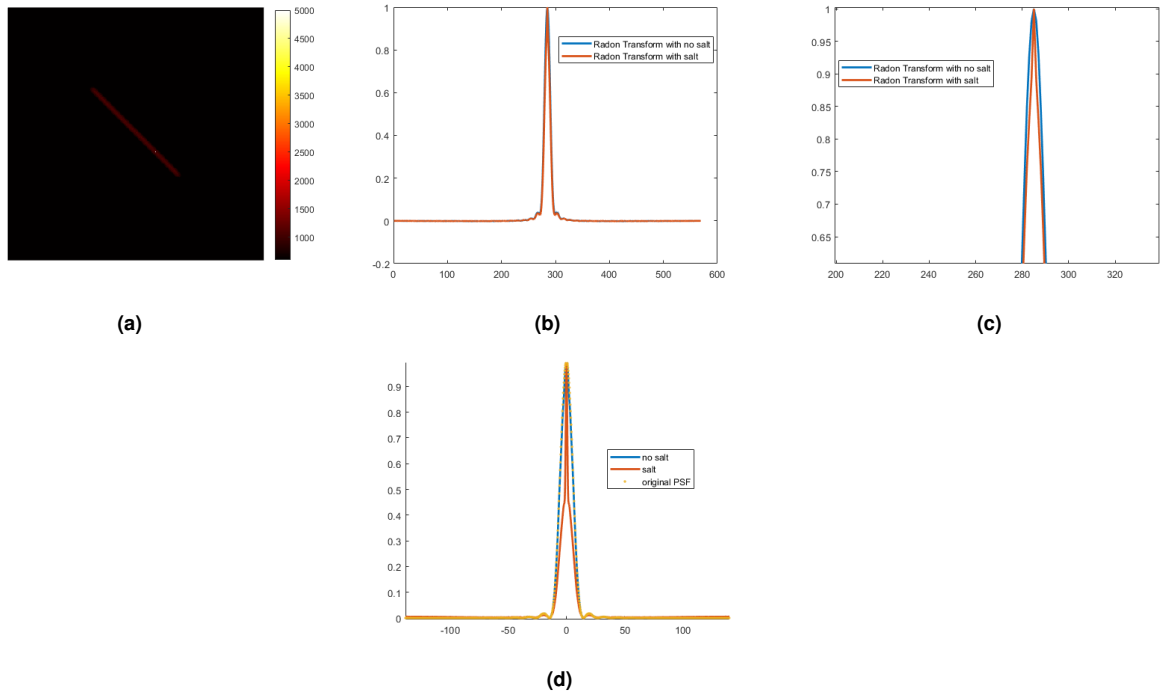


Fig. 9. (a) : Synthetic image of a LSF with a 45° of inclination, with background= 50, Poisson noise (maximum intensity= 1000) and a salt pixel. (b): Normalized Radon transform of (a) and of the image in Figure 8a. (c): zoom around the peak of (b). (d): profile of the PSF- Radon compared with the PSF- Radon function obtained in Figure 8d.

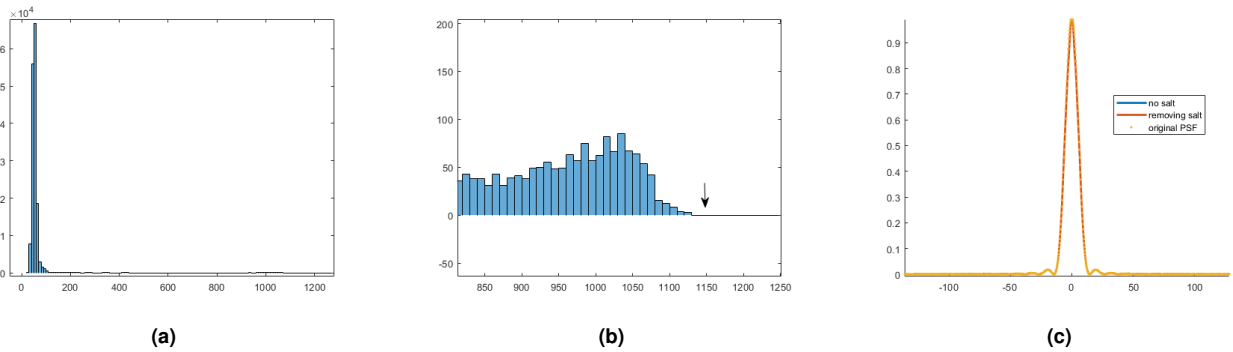


Fig. 10. (a) : Histogram of the image on Figure 9a. (b) is a zoom of the histogram around the zone corresponding to the intensities of the sample. The arrow in (b) indicates the threshold given by Algorithm 3. (c) comparison between the PSF-Radon functions obtained removing the salt noise together with the original PSF.

B. Recovering the Radon transform of the LSF from a multiline-SF

When there is no isolated LSF but we have an acquisition of 2 or more lines (see Figure 11a) it is necessary to subtract the contribution of the second line. We call a structure of this form a n-Line Spread Function (n-LSF). Assume that our structure is such that the Radon transform has the form $f_0(x) = g(x - x_0) + \alpha g(x - x_1)$ (see blue line in Figure 11b), if we define

$$f_1(x) = f_0(x) - \alpha f_0(x - x_1 + x_0) = g(x - x_0) - \alpha^2 g(x - 2x_1 + x_0) = g(x - x_0) - \alpha^2 g(x - x_2) \quad (13)$$

where $x_2 = 2x_1 - x_0$, that is $x_2 - x_0 = 2(x_1 - x_0)$ which means that we are duplicating the distance to x_0 (see red line in Figure 11b). Therefore now the lobes are more separated and the tail due to the lobe centered at x_2 does not affect the lobe centered at x_0 . We define,

$$R_L(x) = \begin{cases} f_1(x) & \text{if } x \leq x_0 \\ f_1(-x) & \text{if } x > x_0. \end{cases} \quad (14)$$

See yellow line in Figure 11b.

Summing, the steps to obtain the Radon transform of a LSF from a n-LSF are defined in Algorithm 4.

Algorithm 4. Radon transform of a LSF from the n-LSF

- 1: **procedure** $R_L(\text{Image})$
- 2: Calculate the Radon transform of the image
- 3: Find the positions of the first peaks and the relative intensity α .
- 4: Calculate f_1
- 5: **return** R_L as in Eq. (14)

In Figure 11 we show, for a synthetic image how is the performance of the method described in Algorithm 4 in the case where the PSF is an Airy2 function and using an image of a two parallel lines which are at distance near the resolution. In this synthetic image the resolution is 480nm and the distance between lines is 500nm . The relative intensities between the two lines is 2. Observe that the retrieval PSF recovers the information of the halo with an error around 1%.

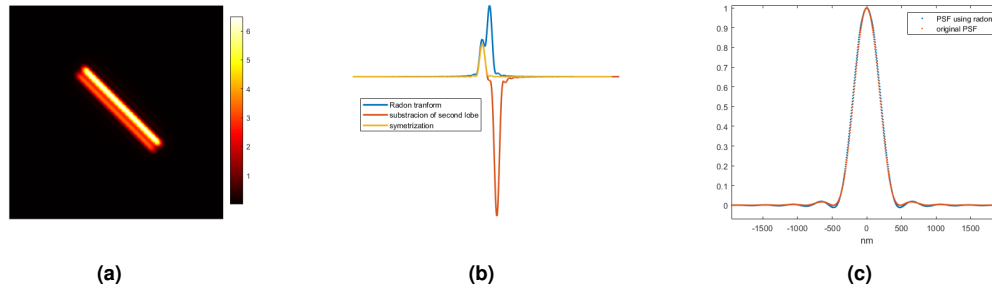


Fig. 11. PSF-Radon using a 2-LSF (a): Original image. (b): Radon transform (blue line), subtraction of the second lobe (red line) and the approximation of the radon transform of the LSF (yellow line). (c) PSF-Radon vs original PSF.

Remark 5.2 In case that x_2 it is still too close to x_0 we can apply Eq. (13) iteratively obtaining

$$f_{i+1}(x) = f_i(x) - \alpha f_i(x - x_i + x_0) = g(x - x_0) - \alpha^{i+2} g(x - 2x_i + x_0) \quad (15)$$

where $x_{i+1} = 2x_i - x_0$ satisfies $x_{i+1} - x_0 = 2(x_i - x_0)$, i.e. $x_{i+1} - x_0 = 2^i(x_1 - x_0)$. That means that after a finite number of steps the 2 lobes are sufficiently separated so that there is no contribution of the second one to the first one.

Also, it is important to mention that if we have a third peak far from the first one, its effect does not affect what happens near the first peak.

6. BACKMATTER

Funding. This document is the result of the research project funded by Universidad de Buenos Aires (ubacyt 2023 20020220200032BA, PIDAE 2022/41); CONICET (PIP 2021-2024 112202000101184); Agencia Nacional de Promoción Científica y Tecnológica (PICT 2020- SERIEA-00617).

Acknowledgement. We want to thank Micaela Toscani for providing us the Argolight images acquired by her.

Disclosures. The authors declare no conflicts of interest.

Research Highlights.

- Determining the instrument point spread function (PSF) is a key issue.
- Precise PSF determinations are mandatory if image improvement is performed numerically by deconvolution.
- Much less exposure time to achieve the same performance than a measurement of the PSF from a very small bead.
- Does not require having to adjust the PSF by an analytical function to overcome the noise uncertainties.

FULL REFERENCES

- 220
- 221 1. "PSF -Radon transform algorithm, stand alone program," <https://nubesan.dm.uba.ar/d/1098f48385454b8a92c6/>.
- 222 2. K. Rossmann, "Point spread-function, line spread-function, and modulation transfer function: tools for the study of imaging systems," *Radiology* **93**,
- 223 257–272 (1969).
- 224 3. R. W. Cole, T. Jinadasa, and C. M. Brown, "Measuring and interpreting point spread functions to determine confocal microscope resolution and ensure
- 225 quality control," *Nat. protocols* **6**, 1929–1941 (2011).
- 226 4. I. Song, H. Yoo, J. Choo, and D.-G. Gweon, "Measurement of point-spread function (psf) for confocal fluorescence microscopy," in *Advanced Characterization*
- 227 *Techniques for Optics, Semiconductors, and Nanotechnologies II*, vol. 5878 (SPIE, 2005), pp. 368–376.
- 228 5. M. Laasmaa, M. Vendelin, and P. Peterson, "Application of regularized richardson-lucy algorithm for deconvolution of confocal microscopy images,"
- 229 *Biophys. J.* **100**, 139a (2011).
- 230 6. M. Gu, "Three-dimensional space-invariant point-spread function for a single lens," *JOSA A* **12**, 1602–1604 (1995).
- 231 7. D. Sage, L. Donati, F. Soulez, D. Fortun, G. Schmit, A. Seitz, R. Guiet, C. Vonesch, and M. Unser, "Deconvolutionlab2: An open-source software for
- 232 deconvolution microscopy," *Methods* **115**, 28–41 (2017).
- 233 8. J. R. Swedlow, "Quantitative fluorescence microscopy and image deconvolution," *Methods cell biology* **81**, 447–465 (2007).
- 234 9. S. Martínez, M. Toscani, and O. E. Martínez, "Superresolution method for a single wide-field image deconvolution by superposition of point sources," *J.*
- 235 *microscopy* **275**, 51–65 (2019).
- 236 10. M. Toscani, O. E. Martínez, and S. Martínez, "Resolution, accuracy and precision in super-resolved microscopy images using suppose," *Opt. Lasers Eng.*
- 237 **161**, 107337 (2023).
- 238 11. H. Kirshner, F. Aguet, D. Sage, and M. Unser, "3-d psf fitting for fluorescence microscopy: implementation and localization application," *J. microscopy* **249**,
- 239 13–25 (2013).
- 240 12. D. K. Samuylov, P. Purwar, G. Székely, and G. Paul, "Modeling point spread function in fluorescence microscopy with a sparse gaussian mixture: Tradeoff
- 241 between accuracy and efficiency," *IEEE Trans. on Image Process.* **28**, 3688–3702 (2019).
- 242 13. J. Li, F. Xue, and T. Blu, "Fast and accurate three-dimensional point spread function computation for fluorescence microscopy," *JOSA A* **34**, 1029–1034
- 243 (2017).
- 244 14. M. Neil, R. Juškaitis, T. Wilson, Z. Laczik, and V. Sarafis, "Optimized pupil-plane filters for confocal microscope point-spread function engineering," *Opt.*
- 245 *letters* **25**, 245–247 (2000).
- 246 15. K. Becker, S. Saghafi, M. Pende, I. Sabyusheva-Litschauer, C. M. Hahn, M. Foroughipour, N. Jährling, and H.-U. Dodt, "Deconvolution of light sheet
- 247 microscopy recordings," *Sci. reports* **9**, 17625 (2019).
- 248 16. B. Zhang, J. Zerubia, and J.-C. Olivo-Marin, "A study of gaussian approximations of fluorescence microscopy psf models," in *Three-Dimensional and*
- 249 *Multidimensional Microscopy: Image Acquisition and Processing XIII*, vol. 6090 (SPIE, 2006), pp. 104–114.
- 250 17. C. Lefort, E. Chouzenoux, L. Magnol, H. Massias, and J.-C. Pesquet, "Multi-parametric 3d-point-spread function estimation in deep multiphoton microscopy
- 251 with an original computational strategy dedicated to the reconstruction of muscle images," in *Optical Sensing and Detection VI*, vol. 11354 (SPIE, 2020),
- 252 pp. 236–243.
- 253 18. E. Chouzenoux, T. T.-K. Lau, C. Lefort, and J.-C. Pesquet, "Optimal multivariate gaussian fitting with applications to psf modeling in two-photon microscopy
- 254 imaging," *J. Math. Imaging Vis.* **61**, 1037–1050 (2019).
- 255 19. A. Royon and N. Converset, "Quality control of fluorescence imaging systems: a new tool for performance assessment and monitoring," *Optik & Photonik*
- 256 **12**, 22–25 (2017).
- 257 20. W. Liu, H. Duan, D. Zhang, X. Zhang, Q. Luo, T. Xie, H. Yan, L. Peng, Y. Hu, L. Liang *et al.*, "Concepts and application of dna origami and dna self-assembly:
- 258 A systematic review," *Appl. Bionics Biomech.* **2021** (2021).
- 259 21. A. Hertle, "On the problem of well-posedness for the radon transform," in *Mathematical Aspects of Computerized Tomography: Proceedings, Oberwolfach,*
- 260 *February 10–16, 1980*, (Springer, 1981), pp. 36–44.
- 261 22. S. I. Kabanikhin, "Definitions and examples of inverse and ill-posed problems," *J. Inverse Ill-posed Probl.* **16**, 317–357 (2008).
- 262 23. "Argolight, user guide argo-powersim," https://argolight.com/files/Argo-POWER/userguide/Argo-POWER-SIM_v2.0_Userguide_v1.0.pdf,2021.